REVIEW ARTICLE
Iran J Allergy Asthma Immunol
In press.

Key Genes Distinguishing Acute and Chronic Immune Thrombocytopenia Identified Through Bioinformatic Analysis

Shuoshuo Gao[1], Chaoqun Li[2], Dongmei Pan[2], Xi Zhang[2], Xiaoshan Zhao[2], and Hua Xu[1]

[1] Department of Pediatric, The First Affiliated Hospital of Guangzhou University of Traditional Chinese Medicine, Guangzhou, China
[2] College of Traditional Chinese Medicine of The Southern Medical University, Guangzhou, China

Received: 21 August 2026; Received in revised form: 25 April 2026; Accepted: 6 May 2026

ABSTRACT

Immune thrombocytopenia (ITP) is an autoimmune hemorrhagic disorder characterized by reduced platelet counts and impaired platelet production. We used bioinformatic methods to compare whole-blood gene-expression profiles from the GSE23754 dataset across acute (ACU), progressive (PRO), and chronic (CHR) phases of ITP. Pairwise GEO2R analyses identified differentially expressed genes (DEGs), followed by cross-comparison, tissue-specificity analysis, functional enrichment, and protein-protein interaction network analysis. We identified 62 DEGs in ACU versus PRO (2 upregulated and 60 downregulated), 15 in CHR versus PRO (3 upregulated and 12 downregulated), and 26 in ACU versus CHR (1 upregulated and 25 downregulated). Ten downregulated genes, including *SLC25A37*, characterized ACU; 5 upregulated genes, including *VNN1*, characterized PRO; and *ALAS2* and *SLC23A2* characterized CHR. Functional analysis linked ACU primarily to innate immunity, inflammation, and hematopoietic dysfunction, whereas PRO and CHR were more closely associated with metabolic dysregulation. Network analysis highlighted *FCGR2B* in the ACU-to-PRO transition, *ACSL1* in the ACU-to-CHR transition, and the ALAS2-HBG1 interaction in the PRO-to-CHR transition. *ALAS2* was differentially expressed across all 3 stages, supporting its potential as an exploratory biomarker of ITP progression. These stage-specific expression patterns provide a molecular basis for further validation and the development of targeted approaches in ITP.

Keywords: Computational biology; Gene expression profiling; Immune thrombocytopenia; Protein interaction mapping

Corresponding Authors: Hua Xu, MD;
Department of Pediatric, The First Affiliated Hospital of Guangzhou University of Traditional Chinese Medicine, Guangzhou, China. Tel: (+86 20) 3659 1367, Email: xuhua212@126.com

Xiaoshan Zhao, MD;
College of Traditional Chinese Medicine of The Southern Medical University, Guangzhou, China. Tel: (+86 20) 3659 1367, Email: zhaoxs0609@163.com

The first and second authors contributed equally to this study

Copyright©, Iran J Allergy Asthma Immunol. All rights reserved.

Published by Tehran University of Medical Sciences (http://ijaai.tums.ac.ir)

IN PRESS

INTRODUCTION

Immune thrombocytopenia (ITP) is an autoimmune hemorrhagic disorder characterized by accelerated platelet destruction. The pathophysiology primarily involves 2 mechanisms: 1) antiplatelet autoantibodies (mainly targeting GPIIb/IIIa) mediate platelet phagocytosis and clearance via Fcγ receptors on splenic macrophages[1,2] and 2) antibody- and cell-mediated immune responses impair bone marrow megakaryopoiesis, with cytotoxic T lymphocyte (CTL)-mediated platelet destruction playing a critical role.[2–4] Additionally, platelets contribute to immune dysregulation by promoting inflammatory responses and releasing platelet microparticles (PMPs).[2–4]

Clinical manifestations include bleeding, fatigue, and reduced quality of life.[5] Chronic ITP patients may exhibit greater tolerance to fatigue.[6] The disease is classified into 3 phases: newly diagnosed (<3 months), persistent (3–12 months), and chronic (>12 months).[2] First-line therapies, such as glucocorticoids and intravenous immunoglobulin (IVIg), often fail to achieve sustained remission.[7,8] Patients with persistent or chronic ITP require maintenance therapies, including thrombopoietin receptor agonists (TPO-RAs) and rituximab; however, refractory ITP remains a clinical challenge.

Research on ITP has expanded beyond the traditional mechanisms of antibody-mediated platelet destruction and insufficient platelet production to explore novel immune mechanisms, including T cell-mediated megakaryocyte apoptosis, suppression of thrombopoiesis, and CTL-mediated attack on autologous platelets.[9] The PD-1 pathway has been shown to regulate CTL activity, offering a new direction for immunomodulatory therapy.[10] Emerging treatments such as TPO-RAs, spleen tyrosine kinase (*SYK*) inhibitors, and FcγR inhibitors are under development, though monoclonal antibodies (e.g., rituximab) may induce adverse effects like hypogammaglobulinemia.[11] Despite advances in understanding immune phenomena and thrombopoietin biology, the genetic regulatory mechanisms of ITP remain to be fully elucidated. This study employs bioinformatics approaches to analyze differential gene expression and signaling pathways across distinct pathological stages, aiming to provide a theoretical foundation for targeted therapies.

MATERIALS AND METHODS

Microarray Sequence Data

The microarray expression data were obtained from the Gene Expression Omnibus (GEO) database under accession number GSE23754. This dataset was generated using the GPL10845 SFGF Human 41K cDNA microarray platform and comprises whole-blood transcriptomic profiles of ITP patients at different disease stages (acute, transitional, and chronic phases). The samples included 8 acute-phase (within 6 months of onset), 4 transitional-phase (approximately 6 months post-acute episode), and 14 chronic-phase (more than 12 months after onset) cases.

Differential Gene Expression Analysis

Patients with ITP were classified into 3 disease-stage groups: acute (ACU), progressive (PRO), and chronic (CHR). Differential expression analysis was conducted using the GEO2R web tool available through the GEO database. Briefly, samples from GSE56232 were assigned to the ACU, PRO, and CHR groups within the GEO2R interface, and pairwise comparisons were performed between ACU vs PRO, CHR and PRO, and ACU and CHR. Differentially expressed transcripts were identified using the criteria of $|\log_2 FC| > 1$ and $p < .05$. Transcript annotations in the "NAME" field were recorded as "clone_ID/GeneBank_list/gene_ID/gene_symbol", and clone_ID-to-gene_ID mappings were verified using the NCBI and GenBank databases. Differentially expressed transcripts were then converted into gene-level datasets for cross-comparison. Stage-specific genes were defined as the intersections of the corresponding pairwise DEG sets: ACU-specific genes from ACU–PRO and ACU–CHR, PRO-specific genes from PRO–ACU and PRO–CHR, and CHR-specific genes from CHR–PRO and CHR–ACU. Because the analysis was based on a single GEO dataset generated on the same microarray platform (GPL10845), major cross-platform bias was inherently limited. In addition, GEO2R uses the processed expression matrix provided in GEO, which has generally undergone platform-specific normalization. Therefore, no additional cross-platform correction was applied in the present study. Nevertheless, as with all retrospective analyses of public microarray data, residual batch effects related to sample processing or experimental conditions cannot be completely excluded and should be considered when interpreting the results. Venn diagrams were generated

IN PRESS

using Venny 2.1, and heatmaps were generated using Hiplot.

Analysis of Differential Gene Expression with Organ Specificity

The analysis of organ-specific gene expression and stage-specific differentially expressed genes across 3 representative groups was performed using the BioGPS online resource (http://biogps.org). Genes meeting all of the following criteria were identified as exhibiting high organ specificity: (1) the expression level of the gene in a specific organ exceeded 10 times the median value; and (2) its second-highest expression level was less than one-third of the highest expression level.

Functional Enrichment Analysis of DEGs in Each Group

Functional enrichment analysis of DEGs in each group was performed using DAVID 6.8 and R software (org.Hs.eg.db package), including functional classification, Gene Ontology (GO) analysis (biological processes [BP], cellular components [CC], and molecular functions [MF]), and KEGG pathway analysis. Functional classification covered UP_keywords and UP_SEQ_feature. GO analysis was employed to predict protein functions, while KEGG analysis mapped DEGs to pathways for constructing molecular interaction networks. Protein-protein interaction (BIOGRID_Interaction) and tissue expression (HPA-normal-Tissue) characteristics were simultaneously analyzed. The significance threshold was set at $p<.05$ with ≥37 enriched genes. For the ACU, PRO, and CHR phases in which the number of DEGs was insufficient (<10), single-gene molecular function annotation was alternatively performed for unique genes, encompassing pathways, as well as protein and tissue functions.

PPI Network Analysis of Differentially Expressed Genes in Each Group

The DEGs identified in each group were mapped to a protein-protein interaction (PPI) network. This network was constructed using the STRING database for protein interactions by importing key molecular lists corresponding to the DEGs from each group, with an interaction score threshold set at >0.4. The resulting PPI tables were saved (including only groups with at least 10 DEGs). For each group, a detailed attribute list was generated to annotate the upregulated or downregulated status of the genes. These interaction tables and attribute lists were subsequently imported into Cytoscape software for visualization and network construction. The node with the highest number of adjacent interactions was identified as the hub node. The ranking order of interacting proteins for each DEG was recorded, with higher-ranked interacting proteins more likely to reflect potential pathway mechanisms associated with the pathophysiology of ITP.

Statistical Analysis

All statistical analyses were performed using SPSS (version 26.0) and R software (version 4.4.1), with a statistical significance threshold set at $p<.05$. Normally distributed data were expressed as mean ± standard deviation (SD), and intergroup comparisons were conducted using Student *t*-test or one-way analysis of variance (ANOVA). Non-normally distributed data were presented as median (interquartile range) [M (P_{25}–P_{75})] and analyzed using the Mann-Whitney U test. Correlation analyses were performed using either Pearson correlation coefficient (for normally distributed data) or Spearman correlation coefficient (for non-normally distributed data), depending on the data distribution.

RESULTS

This study utilized the microarray expression dataset GSE23754 from the GEO database. DEGs at different disease stages of ITP patients were analyzed using the online analytical tool GEO2R. The comparative results of DEGs across various pathological stages of ITP are presented as follows. The DEG profiles between ACU and PRO are illustrated in Figure 1A, revealing 2 upregulated DEGs and 60 downregulated DEGs.

IN PRESS

Published by Tehran University of Medical Sciences (http://ijaai.tums.ac.ir)

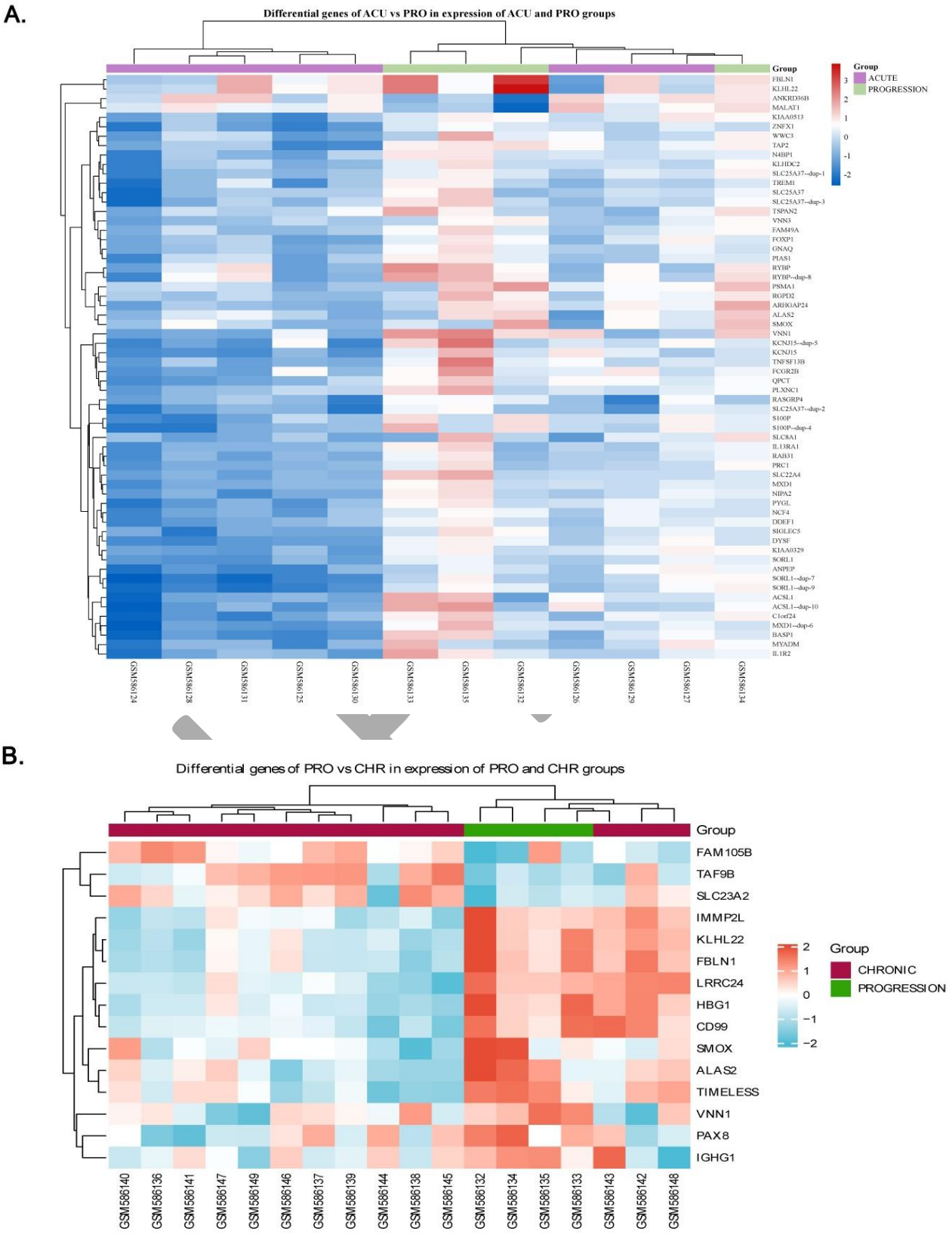
A.
Differential genes of ACU vs PRO in expression of ACU and PRO groups
Group
ACUTE
PROGRESSION
FBLN1
KLHL22
ANKRD36B
MALAT1
KIAA0513
ZNFX1
WWC3
TAP2
N4BP1
KLHDC2
SLC25A37--dup-1
TREM1
SLC25A37
SLC25A37--dup-3
TSPAN2
VNN3
FAM49A
FOXP1
GNAQ
PIAS1
RYBP
RYBP--dup-8
PSMA1
RGPD2
ARHGAP24
ALAS2
SMOX
VNN1
KCNJ15--dup-5
KCNJ15
TNFSF13B
FCGR2B
QPCT
PLXNC1
RASGRP4
SLC25A37--dup-2
S100P
S100P--dup-4
SLC8A1
IL1RA1
RAB31
PRC1
SLC22A4
MXD1
NIPA2
PYGL
NCF4
DDEF1
SIGLEC5
DYSF
KIAA0329
SORL1
ANPEP
SORL1--dup-7
SORL1--dup-9
ACSL1
ACSL1--dup-10
C1orf24
MXD1--dup-6
BASP1
MYADM
IL1R2
GSM586124
GSM586128
GSM586131
GSM586125
GSM586130
GSM586133
GSM586135
GSM586132
GSM586126
GSM586129
GSM586127
GSM586134
B.
Differential genes of PRO vs CHR in expression of PRO and CHR groups
Group
FAM105B
TAF9B
SLC23A2
IMMP2L
KLHL22
FBLN1
LRRC24
HBG1
CD99
SMOX
ALAS2
TIMELESS
VNN1
PAX8
IGHG1
Group
CHRONIC
PROGRESSION
GSM586140
GSM586136
GSM586141
GSM586147
GSM586149
GSM586146
GSM586137
GSM586139
GSM586144
GSM586138
GSM586145
GSM586132
GSM586134
GSM586135
GSM586133
GSM586143
GSM586142
GSM586148

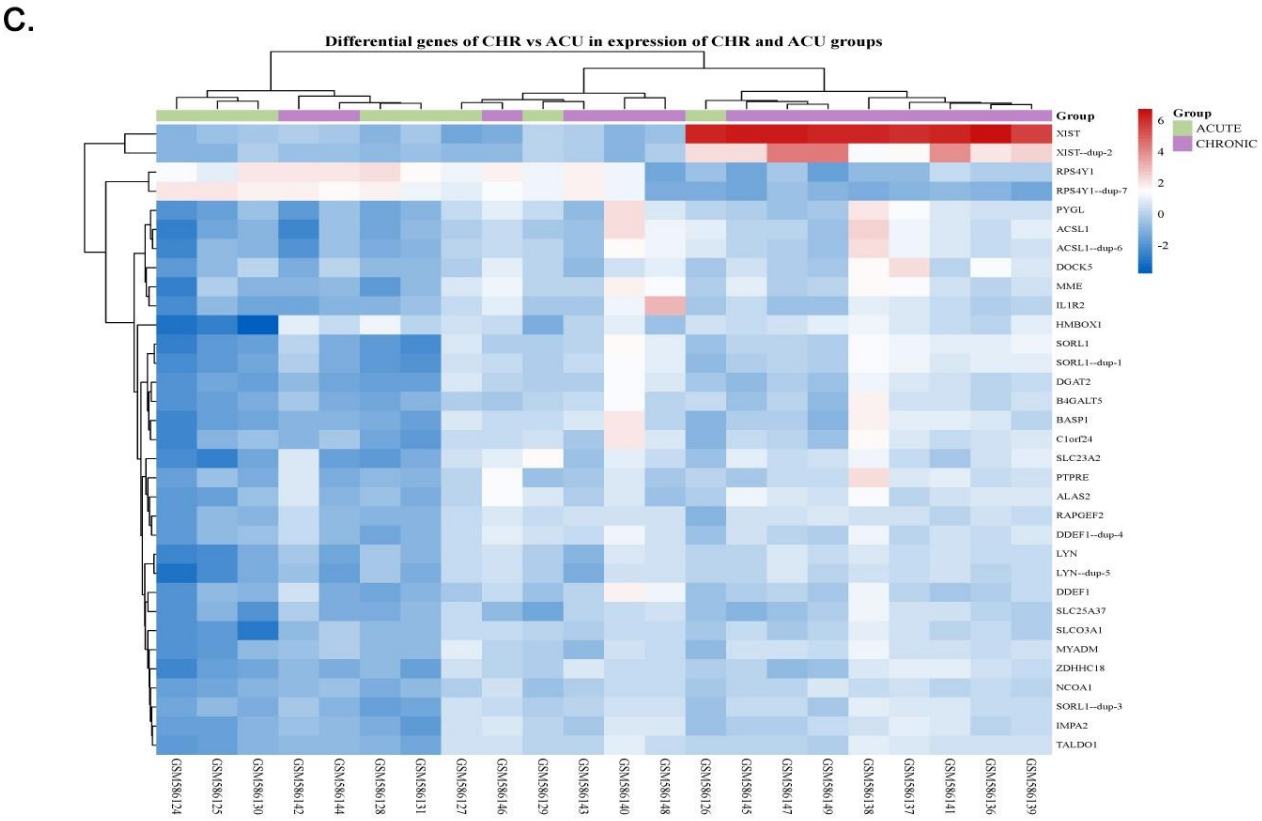

Figure 1. Analysis of DEGs through pairwise comparison of three representative groups. (A) Analysis of DEGs through pairwise comparison of three representative groups. A heat map of differentially expressed genes of ACU vs PRO in both groups including 12 samples. (B) A heat map of differentially expressed genes of PRO vs CHR in both groups including 18 samples. (C) A heat map of differentially expressed genes of CHR vs ACU in both groups including 22 samples. Red represents up-regulated genes; Blue represents down-regulated genes.

Among these DEGs, *ANKRD36B* was upregulated in ACU, predominantly distributed in plasma and blood cells, and closely associated with immune regulation. The non-coding RNA gene *MALAT1* participates in multi-gene regulation and cell cycle modulation and is functionally linked to tumor proliferation and metastasis. The remaining downregulated genes primarily exhibited the following functional characteristics: Immune system-related genes including *VNN* family, *KLHL22*, *TAP2*, *MYADM*, *FCGR2B*, *TREM1*, *PLXNC1*, *PIAS1*, *IL13RA1*, *RGPD2*, *NCF4*, *KIAA0329*, and *SORL1*. Protein phosphorylation and ubiquitination regulatory genes including *BASP1* and *KLHDC2*. Cell cycle/division/proliferation/apoptosis, cytoskeletal remodeling, and membrane ion exchange-related genes including *ASAP1*, *NIBAN1*, *KCNJ15*, *ARHGAP24*, *NIPA2*, *S100P*, *SLC22A4*, *TSPAN2*, and *SLC8A1*. Hematologic malignancy-associated genes including *RYBP*, *TNFSF13B*, and *MXD1*. Platelet adhesion-related gene included *FBLN1*. Tissue-specific protein genes including *DYSF*, *SIGLEC5*, and *KIAA0513*. Mitochondrial and other organelle-related genes including*SLC25A37* and *ALAS2*. Substance and energy metabolism, and synthetase-related genes including *ACSL1*, *N4BP1*, *QPCT*, *PSMA1*, *PYGL*, *RASGRP4*, *SMOX*, *ANPEP*, and *WWC3*. Protein translation/transcription factor synthesis and transcriptional regulation genes including *FOXP1*, *ZNFX1*, and *GNAQ*.

The DEG profiles between the CHR and PRO groups are presented in Figure 1B, revealing 3 upregulated DEGs and 12 downregulated DEGs. The upregulated DEGs included *OTULIN*, *SLC23A2*, and *TAF9B*. The downregulated genes comprised hematopoietic tissue- and immune system-related genes (*IGHG1*, *CD99*, *HBG1*, *VNN* family, and *FBLN1*); an isoenzyme synthesis and cellular function-related gene (*SMOX*); organelle function-related genes (*IMMP2L* and *ALAS2*);

Published by Tehran University of Medical Sciences (http://ijaai.tums.ac.ir)

a tissue development-related gene (*PAX8*); a cellular damage response gene (*TIMELESS*); and a cell membrane structure and synapse formation gene (*LRRC24*).

The DEG profiles between the ACU and CHR groups are presented in Figure 1C, revealing 1 upregulated DEG and 25 downregulated DEGs. The upregulated DEG was *RPS4Y1*, which is involved in autoimmune diseases. The main functions of the 25 relatively downregulated DEGs (with repetitive DNA genes counted only once) included transcription factors involved in transcriptional regulation, protein translation, synthesis, protein phosphorylation, and ubiquitination (*NCOA1*, *BASP1*, *HMBOX1*, and *XIST*), enzymes involved in the synthesis of biological compounds and participating in the metabolism of substances and energy in the body (*B4GALT5*, *LYN*, *TALDO1*, *PYGL*, *ZDHHC18*, *DGAT2*, *IMPA2*, *ACSL1*, and *ALAS2*), genes related to the transport of substances across cell membranes, ion exchange, cell division, proliferation, apoptosis, and cytoskeletal remodeling (*ASAP1*, *NIBAN1*, *DOCK5*, *PTPRE*, *RAPGEF2*, *SLCO3A1*, *SLC23A2*, and *SLC25A37*), and genes associated with hematopoiesis, the immune system, humoral immunity, cellular immunity, and the migration and transport (*MYADM*, *IL1R2*, *SORL1*, and *MME*).

Pairwise Comparison of DEGs Among Groups to Identify Unique DEGs of ITP at Different Stages

By performing a cross-analysis of the DEGs identified in the pairwise comparisons, we further elucidated the unique differential genes specific to various stages of ITP. The proteins encoded by these unique differential genes are likely to serve as biomarkers for ITP at their respective pathological stages. The DEGs specific to the ACU phase were identified through a cross-analysis of the DEGs from pairwise comparisons of ACU vs PRO and ACU vs CHR samples. A Venn diagram (Figure 2A) ultimately identified 10 downregulated overlapping DEGs, which were confirmed as acute-phase-specific differential genes.

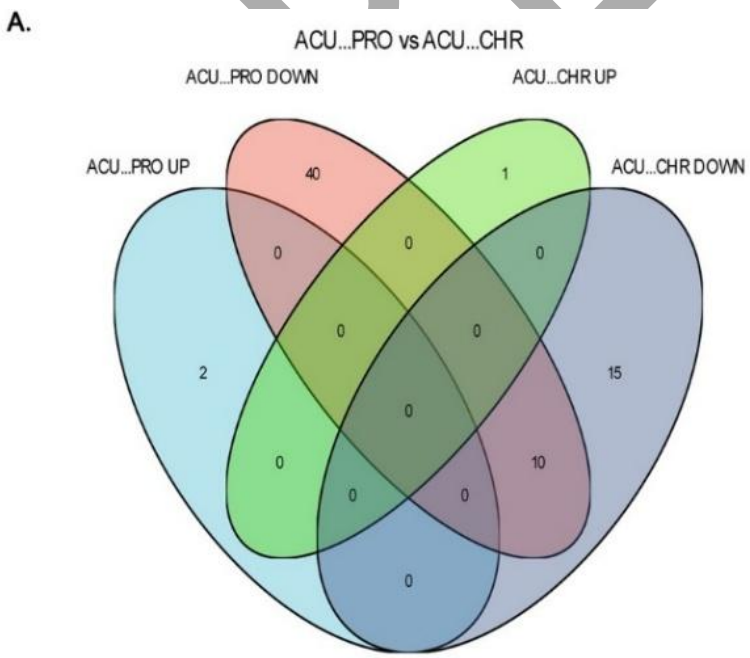

B.

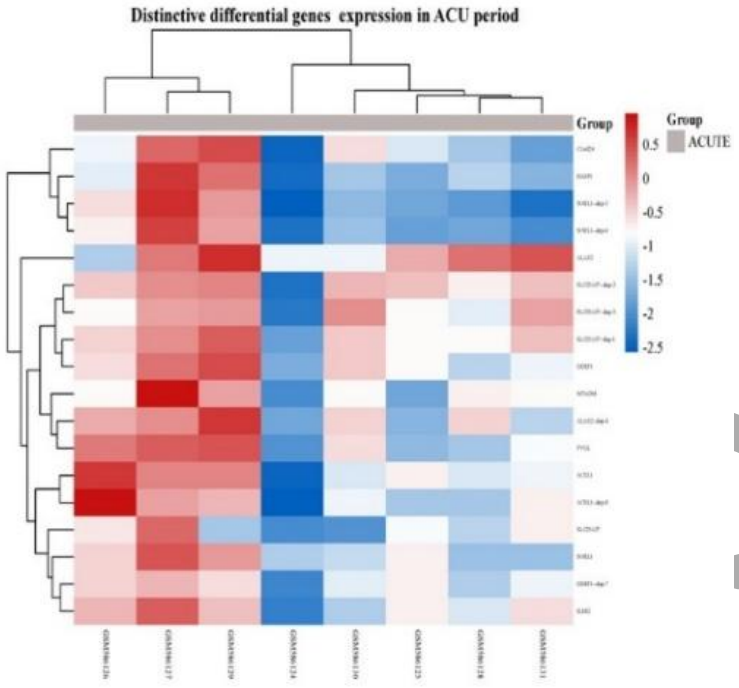

C.

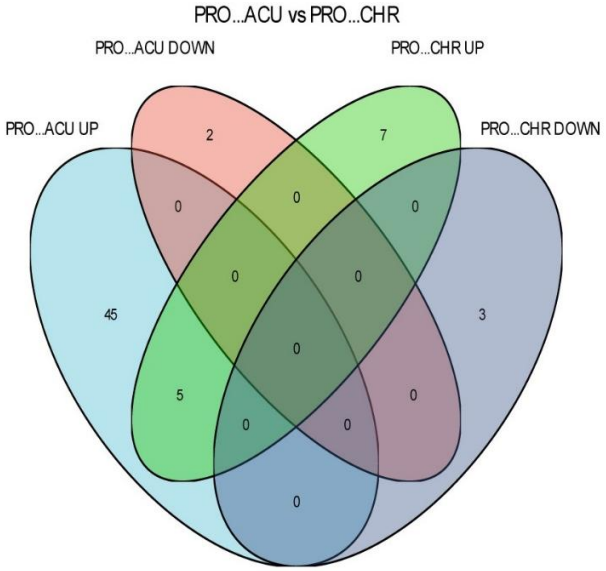

Published by Tehran University of Medical Sciences (http://ijaai.tums.ac.ir)

D.

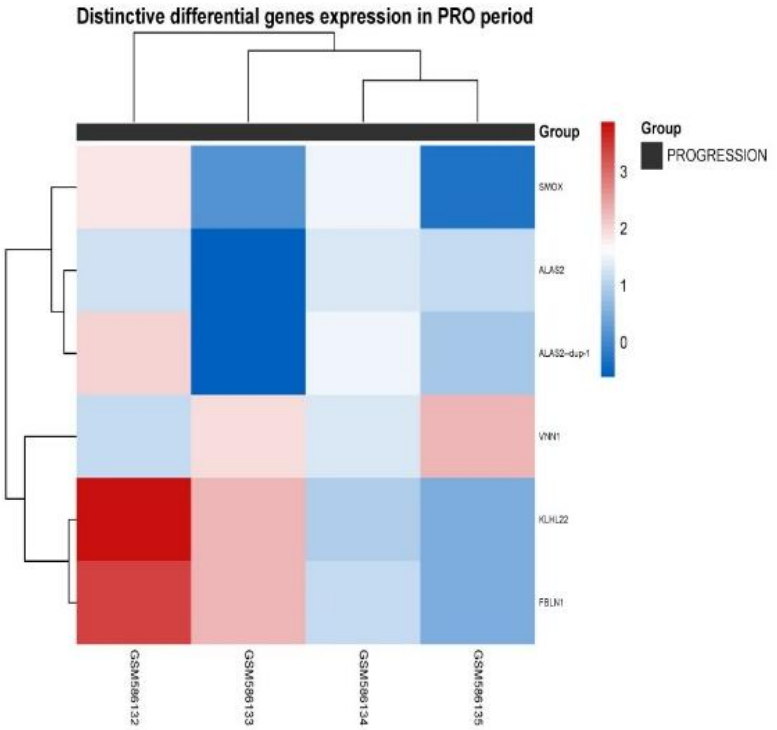
Distinctive differential genes expression in PRO period
Group
Group
PROGRESSION
3
2
1
0
SMOX
ALAS2
ALAS2-dup-1
VNN1
KLHL22
FBLN1
GSM586132
GSM586133
GSM586134
GSM586135

E.

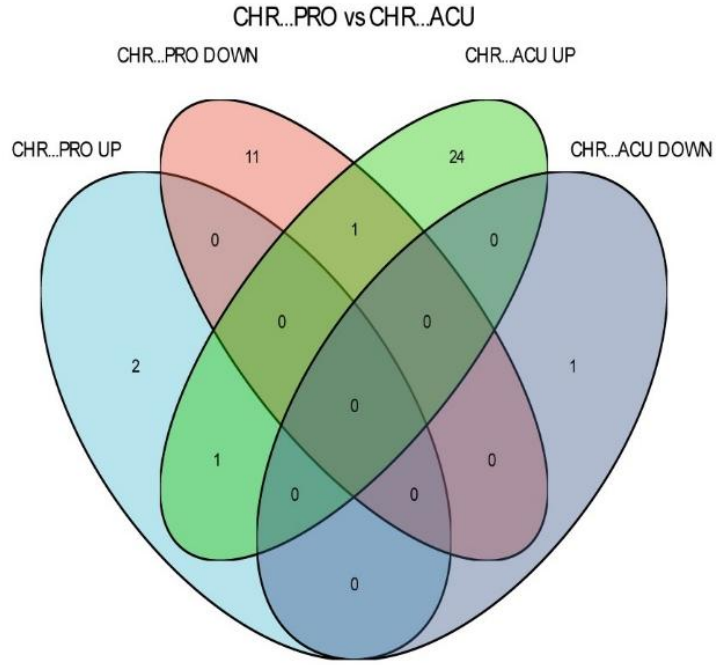
CHR...PRO vs CHR..ACU
CHR...PRO DOWN
CHR...ACU UP
CHR...PRO UP
CHR...ACU DOWN
11
24
2
1
0
1
0
0
0
0
1
0
0
0
0
0

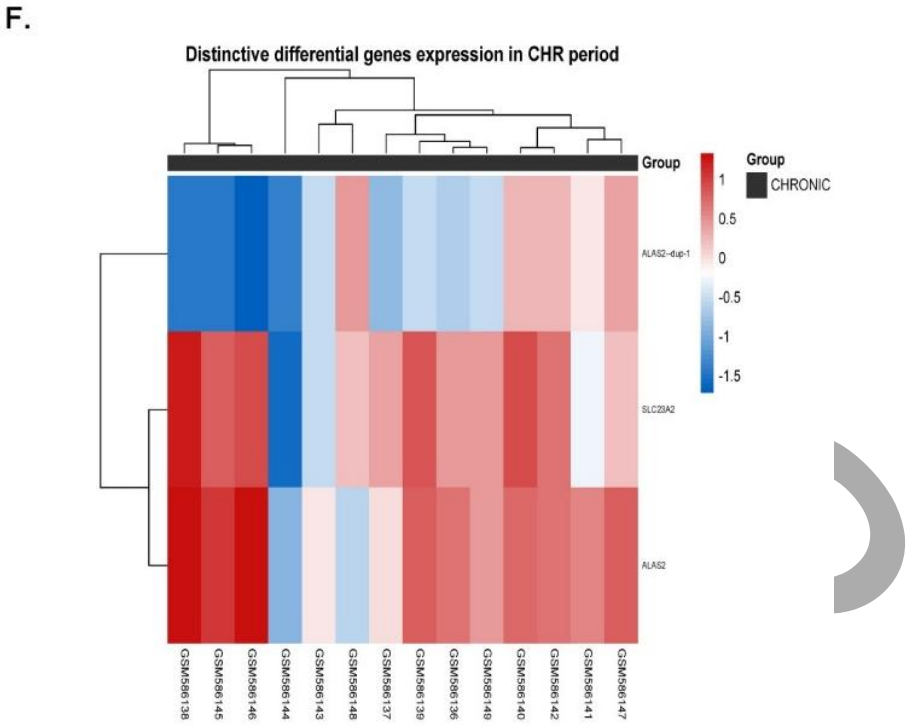

Figure 2. Pairwise Comparison of DEGs Among Groups to Identify Unique Differential Genes of ITP at Different Stages. (A) Venn diagram shows overlap of differential genes of ACU-PRO vs ACU-CHR groups to determine distinctive differential genes in ACU period. ("UP" means up-regulated genes; "DOWN" means down-regulated genes). (B) The heat map of distinctive differential genes expression in ACU period including 8 samples. (C) Venn diagram shows overlap of differential genes of PRO-ACU vs PRO-CHR groups to determine distinctive differential genes in PRO period. (D) The heat map of distinctive differential genes expression in PRO period including 4 samples. (E) Venn diagram shows overlap of differential genes of CHR-ACU vs CHR-PRO groups to determine distinctive differential genes in CHR period. (F) The heat map of distinctive differential genes expression in CHR period including 14 samples.

The heatmap (Figure 2B) illustrates the expression levels of these 10 unique DEGs across various samples during the ACU phase of ITP. The DEGs specific to the PRO phase were identified through a comparative analysis of the DEGs from the PRO vs ACU and the DEGs from the PRO vs CHR samples. A Venn diagram (Figure 2C) ultimately identified 5 upregulated overlapping DEGs, which were determined to be unique differential genes specific to the PRO phase of ITP. A heatmap (Figure 2D) illustrates the expression levels of these 5 unique DEGs across various samples during the PRO phase of ITP. The DEGs unique to the CHR stage were identified through cross-analysis of DEGs obtained from pairwise comparisons between CHR vs ACU samples and between CHR vs PRO samples. A Venn diagram (Figure 2E) ultimately revealed 2 overlapping differential genes. Among these, *SLC23A2* exhibited upregulation at the same RNA transcription site, whereas *ALAS2* had 2 distinct RNA transcription sites, one upregulated and the other downregulated. These 2 overlapping DEGs were confirmed as stage-specific DEGs during the chronic phase of ITP. The heatmap (Figure 2F) illustrates the expression levels of these 2 unique DEGs across various samples during the CHR stage of ITP.

Identification of Tissue-specific Expression of DEGs in ITP

BioGPS was used to identify the expression patterns of DEGs associated with ITP in specific tissues or organ systems at different stages. Three representative groups and 3 pathological stages were screened for DEGs based on stringent criteria for high tissue specificity. The findings revealed that these highly tissue-specific DEGs were predominantly expressed in the circulatory system, immune system, musculoskeletal system, connective

tissues, and nervous system. In the comparison between the ACU and PRO groups, 8 DEGs exhibiting high tissue-specific expression were identified. Among these, the genes primarily associated with the blood and immune system included *SLC25A37*, *ALAS2*, *MXD1*, *PLXNC1*, *MYADM*, *SLC22A4*, and *SORL1*. The distribution of these 8 DEGs across highly expressed specific tissues and organs is shown in Figure 3A .

Seven DEGs with highly tissue-specific differential expression were identified in the ACU-versus-CHR comparison. Genes predominantly expressed in the hematologic and immune systems included *MYADM*, *SORL1*, *ZDHHC18*, and *ALAS2*; *DGAT2* and *MME* were mainly expressed in the musculoskeletal and connective-tissue systems, and *SLC23A2* was mainly expressed in the nervous system. Their tissue distribution is shown in Figure 3B. Two highly tissue-specific DEGs were identified in the CHR-versus-PRO comparison: *ALAS2* in the hematologic and immune systems and *SLC23A2* in the nervous system. Their tissue distribution is shown in Figure 3C.

Four genes (*SLC25A37*, *ALAS2*, *SORL1*, and *MYADM*) predominantly exhibiting highly tissue-specific expression during the ACU phase were identified among the unique DEGs, and they were distributed within the hematopoietic immune system. The distribution pattern of these 4 genes was shown in Figure 3D. Among the unique DEGs with highly tissue-specific expression identified during the PRO phase, 1 gene was primarily identified, *ALAS2*. The distribution pattern of this gene was shown in Figure 3E. Among the characteristic DEGs exhibiting highly tissue-specific expression during the CHR phase, 2 genes (*ALAS2* and *SLC23A2*) were predominantly identified. These genes are distributed respectively within the hematopoietic immune system and the nervous system (Figure 3F).

A.

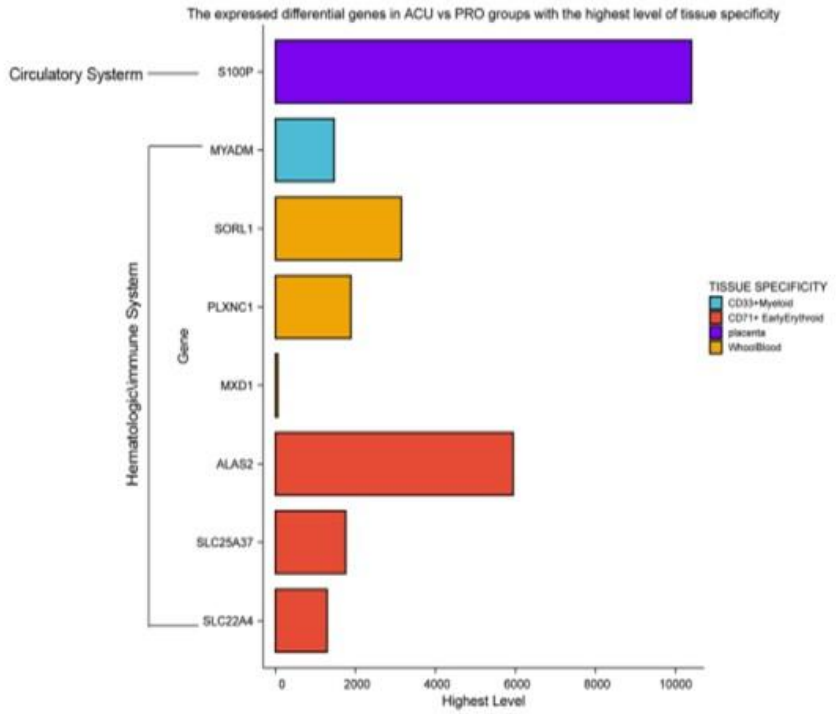

Published by Tehran University of Medical Sciences (http://ijaai.tums.ac.ir)

B.

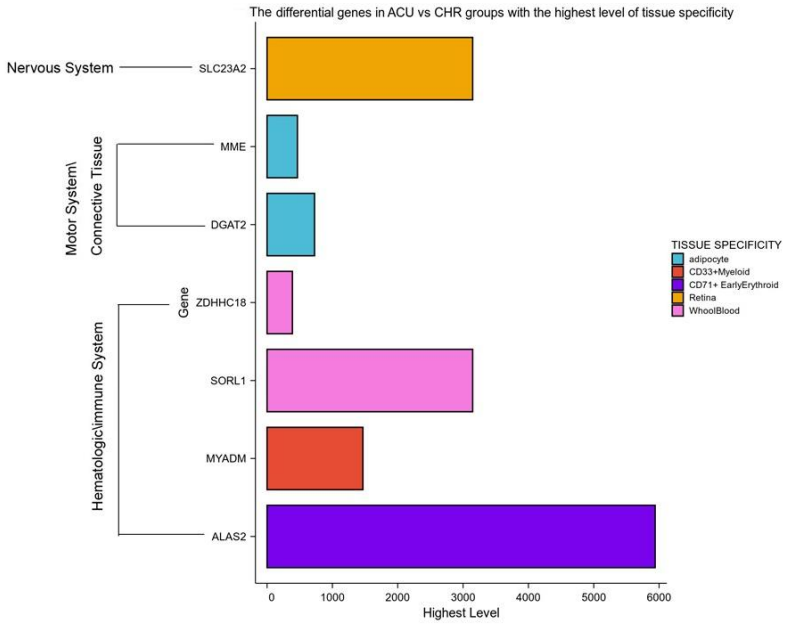
The differential genes in ACU vs CHR groups with the highest level of tissue specificity
Nervous System
SLC23A2
Motor System\ Connective Tissue
MME
DGAT2
Gene
Hematologic\immune System
ZDHHC18
SORL1
MYADM
ALAS2
TISSUE SPECIFICITY
adipocyte
CD33+Myeloid
CD71+ EarlyErythroid
Retina
WhoolBlood
0
1000
2000
3000
4000
5000
6000
Highest Level

C.

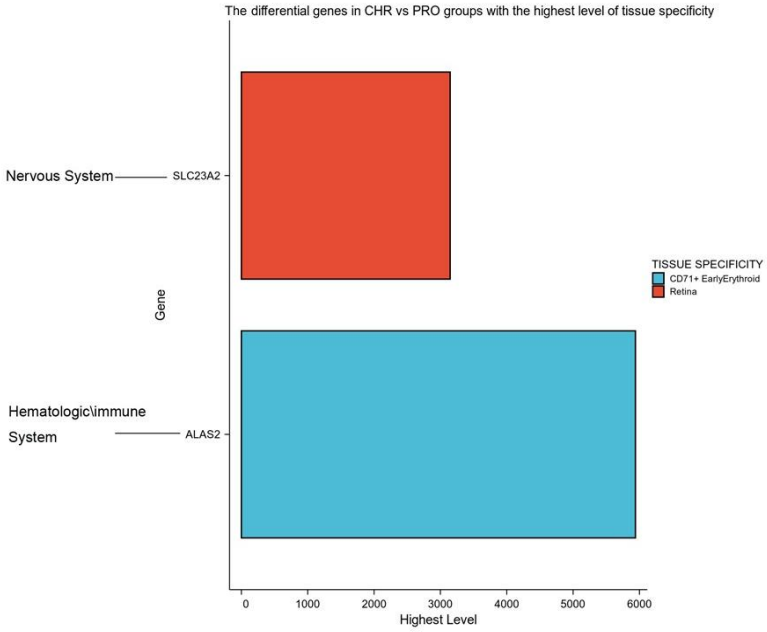
The differential genes in CHR vs PRO groups with the highest level of tissue specificity
Nervous System
SLC23A2
Gene
Hematologic\immune System
ALAS2
TISSUE SPECIFICITY
CD71+ EarlyErythroid
Retina
0
1000
2000
3000
4000
5000
6000
Highest Level

D.

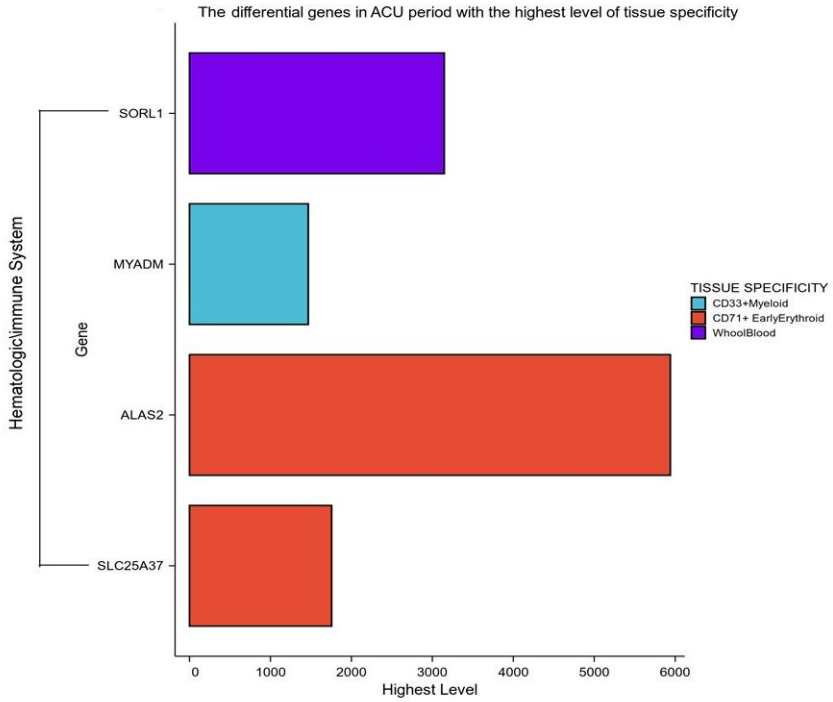
The differential genes in ACU period with the highest level of tissue specificity
SORL1
MYADM
ALAS2
SLC25A37
Gene
Hematologic\Immune System
TISSUE SPECIFICITY
CD33+Myeloid
CD71+ EarlyErythroid
WhoolBlood
0
1000
2000
3000
4000
5000
6000
Highest Level

E.

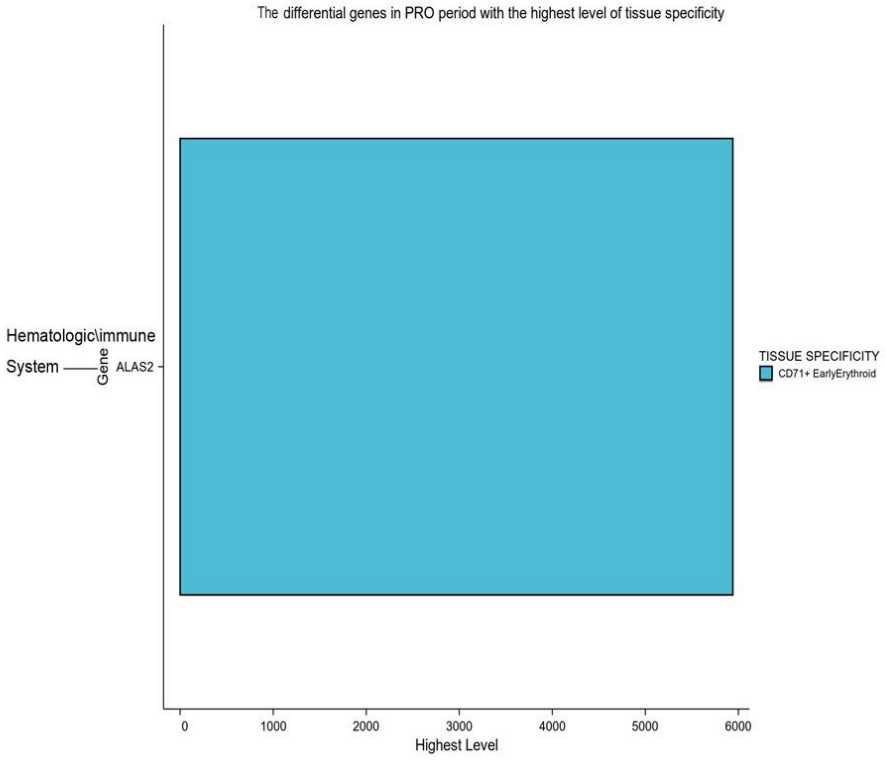
The differential genes in PRO period with the highest level of tissue specificity
Hematologic\Immune System
Gene
ALAS2
TISSUE SPECIFICITY
CD71+ EarlyErythroid
0
1000
2000
3000
4000
5000
6000
Highest Level

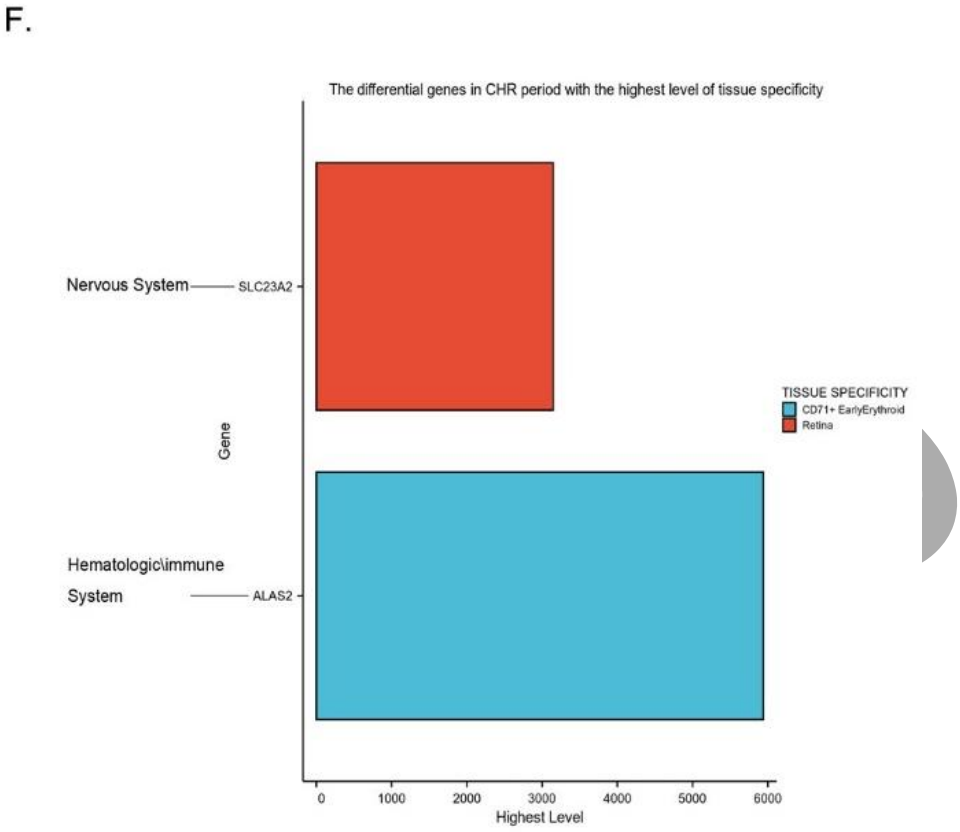

Figure 3. Identification of tissue-specific expression of DEGs in ITP. Bar graphs of differentially expressed genes with tissue specificity. (A) In ACU VS PRO groups. (B) In ACU VS CHR groups. (C) In CHR VS PRO groups. (D) In ACU period. (E) In PRO period. (F) In CHR period.

Functional Enrichment Analysis of DEGs in each Group

The study employed DAVID in conjunction with R software to perform functional enrichment analysis on the DEGs between the ACU vs PRO groups, ACU vs CHR groups, and CHR vs PRO groups. The enrichment analysis included Gene Ontology (GO) analysis, Kyoto Encyclopedia of Genes and Genomes (KEGG) pathway analysis, functional classification, protein interactions, and aggregated tissue and organ data.

In the functional enrichment analysis of DEGs between the ACU and PRO groups, the biological process (BP) category involved 11 relevant genes. The cellular component (CC) category involved 26 relevant genes. The molecular function (MF) category involved 19 relevant genes. Proteins interacting with the DEGs were enriched, resulting in 14 identified interactions involving 30 interacting DEGs. Figure 4A illustrates the enrichment analysis of DEGs between ACU and PRO across 5 functional categories, encompassing a total of 33 functional items.

Published by Tehran University of Medical Sciences (http://ijaai.tums.ac.ir)

A.

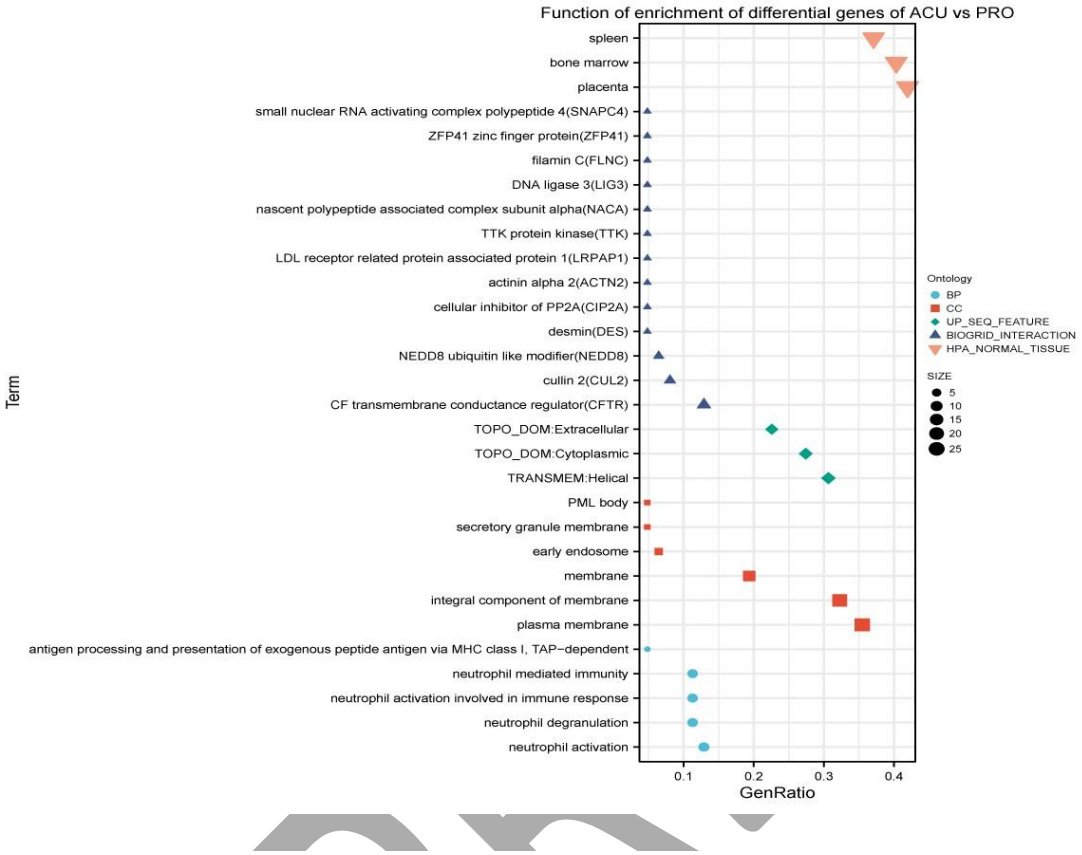
Function of enrichment of differential genes of ACU vs PRO
spleen
bone marrow
placenta
small nuclear RNA activating complex polypeptide 4(SNAPC4)
ZFP41 zinc finger protein(ZFP41)
filamin C(FLNC)
DNA ligase 3(LIG3)
nascent polypeptide associated complex subunit alpha(NACA)
TTK protein kinase(TTK)
LDL receptor related protein associated protein 1(LRPAP1)
actinin alpha 2(ACTN2)
cellular inhibitor of PP2A(CIP2A)
desmin(DES)
NEDD8 ubiquitin like modifier(NEDD8)
cullin 2(CUL2)
CF transmembrane conductance regulator(CFTR)
TOPO_DOM:Extracellular
TOPO_DOM:Cytoplasmic
TRANSMEM:Helical
PML body
secretory granule membrane
early endosome
membrane
integral component of membrane
plasma membrane
antigen processing and presentation of exogenous peptide antigen via MHC class I, TAP−dependent
neutrophil mediated immunity
neutrophil activation involved in immune response
neutrophil degranulation
neutrophil activation
Term
0.1
0.2
0.3
0.4
GenRatio
Ontology
BP
CC
UP_SEQ_FEATURE
BIOGRID_INTERACTION
HPA_NORMAL_TISSUE
SIZE
5
10
15
20
25

B.

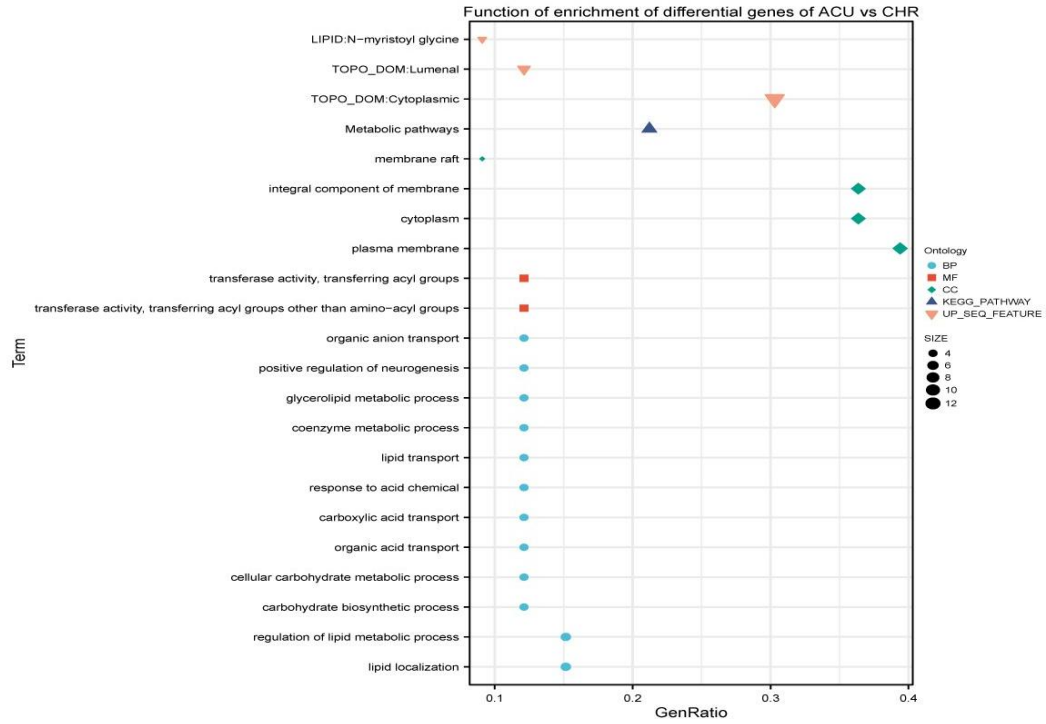
Function of enrichment of differential genes of ACU vs CHR
LIPID:N−myristoyl glycine
TOPO_DOM:Lumenal
TOPO_DOM:Cytoplasmic
Metabolic pathways
membrane raft
integral component of membrane
cytoplasm
plasma membrane
transferase activity, transferring acyl groups
transferase activity, transferring acyl groups other than amino−acyl groups
organic anion transport
positive regulation of neurogenesis
glycerolipid metabolic process
coenzyme metabolic process
lipid transport
response to acid chemical
carboxylic acid transport
organic acid transport
cellular carbohydrate metabolic process
carbohydrate biosynthetic process
regulation of lipid metabolic process
lipid localization
Term
0.1
0.2
0.3
0.4
GenRatio
Ontology
BP
MF
CC
KEGG_PATHWAY
UP_SEQ_FEATURE
SIZE
4
6
8
10
12

C.

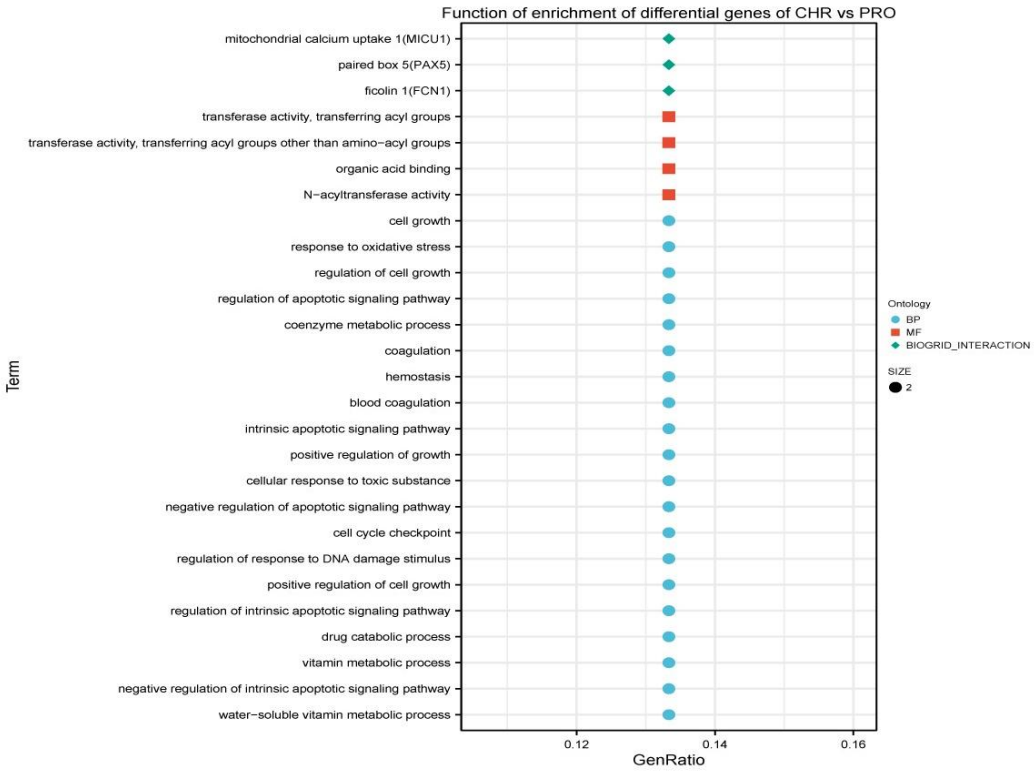

Figure 4. Functional enrichment analysis of DEGs in each group. Point graphs of function of enrichment of differentially expressed genes. (A) In ACU VS PRO groups. (B) In ACU VS CHR groups. (C) In CHR VS PRO groups.

During the functional enrichment analysis of DEGs between the ACU and CHR groups, the BP encompassed 24 DEGs. The MF mainly focused on 4 DEGs. Regarding CC, 20 related DEGs were identified. Enrichment analysis revealed 1 KEGG pathway associated with metabolic processes, involving 7 related DEGs. Protein interaction analysis of the DEGs yielded 21 interacting proteins, with 20 interacting DEGs identified. The tissues and organs associated with these DEGs were primarily the placenta, with 13 related genes identified. Figure 4B displays the identification of 22 functional items from 5 categories within the 11 enriched functions, focusing on the DEG enrichment between ACU and CHR.

During the functional enrichment analysis of DEGs between the CHR and PRO groups, the BP encompassed 16 DEGs. The MF mainly concentrated on 3 related DEGs (*ALAS2*, *TAF9B*, and *HBG1*). Additionally, 3 proteins interacting with the DEGs were enriched, with 4 interacting DEGs (*FBLN1*, *KLHL22*, *PAX8*, and *IMMP2L*). Figure 4C illustrates the enrichment analysis of 27 functional items across 3 categories in the GO analysis comparing CHR vs PRO.

PPI Interaction Network Analysis of Differential Genes in Each Group

The DEGs in each group were mapped using the STRING PPI database, with an interaction score threshold set at greater than 0.4, resulting in a protein interaction table for the differential genes of each group. By combining the lists of upregulated and downregulated DEGs, the data were imported into Cytoscape software for visualization and construction of the PPI network. The analysis focused on the interaction frequency of differential proteins with adjacent proteins within each group's PPI network, allowing for the ranking of the top hub genes among these interacting differential genes in the PPI network.

Among the DEGs identified between ACU and PRO, 12 genes were associated with the formation of the

Published by Tehran University of Medical Sciences (http://ijaai.tums.ac.ir)

PPI interaction network, including *VNN1*, *VNN3*, *ALAS2*, *SLC25A37*, *FCGR2B*, *TNFSF13B*, *TREM1*, *IL1R2*, *NCF4*, *ANPEP*, *OBP2B*, and *IL13RA1*. Figure 5A illustrates the interaction relationships among these 12 differential genes, while Figure 5B presents the ranking of the top 8 genes and their interaction relationships.

The central gene with the most connections to adjacent gene nodes is *FCGR2B*, which has the highest rank. The next highest-ranking genes are *TREM1* and *IL1R2*, followed by *NCF4*, *ANPEP*, *VNN1*, *OBP2B*, and *VNN3*, which have the lowest ranks. Among the DEGs identified between ACU and CHR group, 11 genes were associated with the formation of the PPI interaction network, including *MME*, *LYN*, *NCOA1*, *ACSL1*, *ALAS2*, *SLC25A37*, *PYGL*, *TALDO1*, *DGAT2*, *PTPRE*, and *DOCK5*. Figure 5C illustrates the interaction relationships among these 11 DEGs, while Figure 5D displays the ranking of the top 7 genes and their interactions. The gene with the highest connectivity to adjacent gene nodes is *ACSL1*, followed by *NCOA1*, *ALAS2*, *SLC25A37*, *PYGL*, *TALDO1*, and *DGAT2*. Among the DEGs identified in the comparison of CHR and PRO groups, 2 genes are associated with the formation of the PPI interaction network, including *HBG1* and *ALAS2*. Figure 5E illustrates the interaction between these 2 genes. Due to the limited number of DEGs in the comparison between CHR and PRO groups, no significant interacting proteins or central node proteins were identified. Among the DEGs specific to the ACU phase, 2 DEGs are associated with the formation of a PPI interaction network, including *ALAS2* and *SLC25A37*. Figure 5F illustrates their interaction relationship. Due to the limited number of ACU-specific DEGs in ITP, the interacting proteins lack a hierarchical order and do not form a central hub protein. The interaction between *ALAS2* and *SLC25A37* was likely involved in the pathway signaling processes underlying the acute phase of ITP.

Overall, the PPI network analysis of DEGs across study groups revealed distinct molecular signatures during disease progression. The transition from ACU to PRO was characterized by signaling pathways centered on *FCGR2B*. In contrast, the progression from ACU to CHR predominantly involved interaction networks with *ACSL1* as the core component. The transition from PRO to CHR was associated with protein interactions related to the *HBG1–ALAS2* signaling pathway. Notably, ACU exhibited unique PPI interactions, including the *ALAS2–SLC25A37* pairing. Longitudinal analysis demonstrated that *ALAS2–SLC25A37* represented a persistent PPI interaction throughout the acute phase, while *HBG1–ALAS2* emerged as the characteristic interaction during progression from the progressive phase to chronic-phase ITP.

IJAAI PRESS

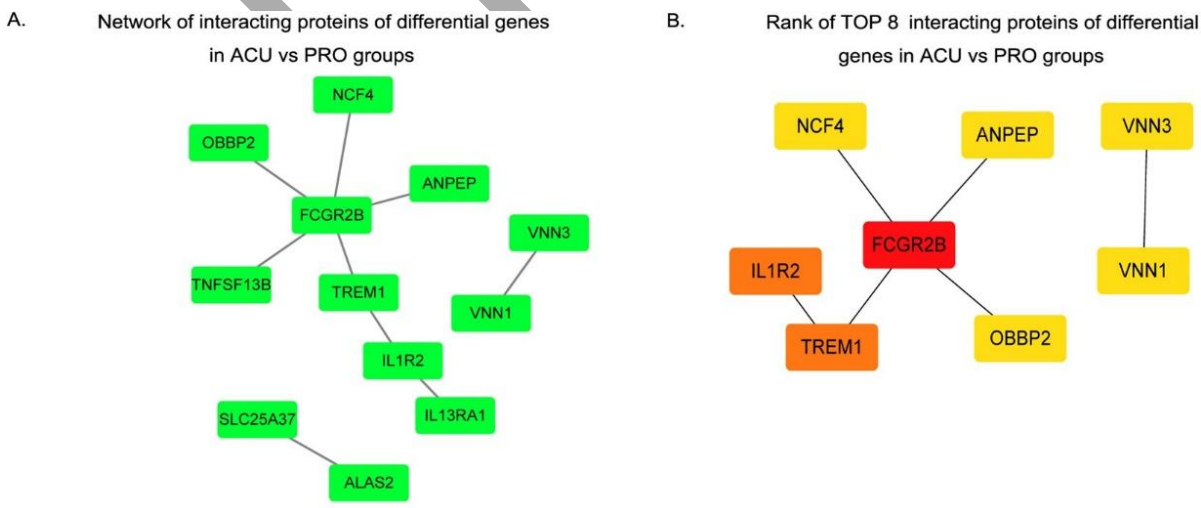

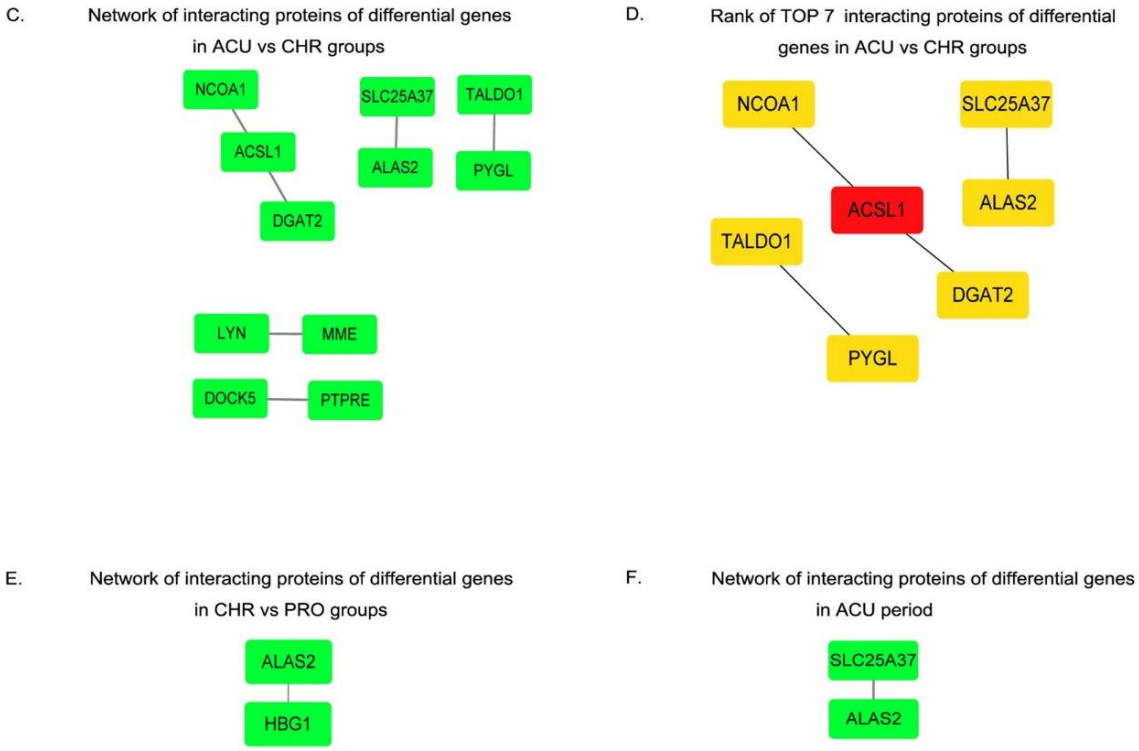

Figure 5. PPI interaction network analysis of DEGs in each group. (A) Network of interacting proteins of differential genes in ACU vs PRO groups. The "GREEN" marks down-regulated genes. (B) Rank of Top 8 interacting proteins of DEGs in ACU vs PRO groups. The "RED" marks the highest rank of interacting proteins of differential genes; The "ORANGE" marks the second highest rank; The "YELLOW" marks the lowest rank). (C) Network of interacting proteins of differential genes in ACU vs CHR groups. (D) Rank of Top 7 interacting proteins of differential genes in ACU vs CHR groups. (E) Network of interacting proteins of differential genes in CHR vs PRO groups. (F) Network of interacting proteins of differential genes in ACU period. The "GREEN" of (C)\(E)\(F) means as same as (A); The rank's color of (D) means as same as (B).

DISCUSSION

Although several laboratory parameters and candidate biomarkers have been explored in ITP, there is still no widely accepted disease-specific molecular marker routinely used in clinical hematology for diagnosis or stage discrimination. Current diagnosis remains largely based on platelet count, bleeding manifestations, exclusion of other causes of thrombocytopenia, and treatment response. In this study, we identified DEGs across pairwise comparisons of the 3 pathological stages of ITP and further characterized stage-specific transcriptional features in ACU, PRO, and CHR. These findings suggest that ITP progression is accompanied by coordinated changes in immune regulation, hematopoietic stress, oxidative balance, and metabolic adaptation.

At the pathway level, several biological processes identified here—including inflammatory immune activation, Fc receptor-related signaling, erythroid and hematopoietic stress responses, oxidative stress, and metabolic dysregulation—are not necessarily unique to ITP and may overlap with mechanisms reported in other autoimmune hematologic disorders. However, because our analysis was designed to compare stages within ITP rather than to directly contrast ITP with other diseases, our results mainly support the conclusion that these immune–hematopoietic programs are organized in a stage-dependent manner during ITP progression. In particular, the involvement of *FCGR2B*, *IL1R2*, and *TREM1* is consistent with broader autoimmune paradigms in which defective inhibitory signaling, excessive myeloid-cell activation, and dysregulated cytokine amplification cooperate to sustain tissue injury.[12–14] This interpretation is also consistent with recent studies in other autoimmune diseases, particularly systemic lupus erythematosus and rheumatoid arthritis, in which impaired inhibitory Fcγ receptor signaling,

persistent cytokine-driven inflammation, and myeloid-cell amplification have all been implicated in loss of immune tolerance and chronic tissue injury. In this context, the transcriptional changes identified here may reflect a shared autoimmune inflammatory framework rather than ITP-specific pathways alone, although their stage-dependent organization may still distinguish ITP progression from other immune-mediated diseases.[15–17]

A prominent acute-phase feature was the downregulation of genes linked to mitochondrial iron handling, immune restraint, and metabolic homeostasis. Among them, *SLC25A37*, which encodes the mitochondrial iron transporter mitoferrin-1, is essential for iron delivery into mitochondria and supports heme synthesis in hematopoietic cells.[18–20] Its downregulation in ACU suggests impaired mitochondrial iron utilization and disturbed erythroid-associated metabolism under inflammatory stress. Because *SLC25A37* function is closely linked to heme production and oxidative metabolism, reduced expression may contribute to disordered aerobic energy metabolism, redox imbalance, and hematopoietic dysfunction during acute disease.[21]

ALAS2 emerged as a stage-spanning gene, being downregulated in ACU, markedly upregulated in PRO, and partially readjusted in CHR. As the erythroid-specific rate-limiting enzyme in heme biosynthesis, *ALAS2* is closely associated with hemoglobin production, erythroid differentiation, mitochondrial iron utilization, and hematopoietic stress responses.[22–24] In inflammatory or infectious conditions, erythroid heme pathways can be remodeled together with immune activation.[25,26] Bioinformatics studies of immune-related and oxidative stress-associated disorders have also identified *ALAS2*-related erythroid or redox signatures, suggesting that *ALAS2* may reflect a broader stress-response program rather than a mechanism unique to ITP.[27–29] Therefore, the recurrent detection of *ALAS2* across all 3 stages may represent a persistent erythropoietic stress axis accompanying disease evolution. In our dataset, loci 435314 and 142087 were reduced in ACU, whereas locus 430077 increased in PRO and decreased again in CHR, suggesting a pattern of acute suppression, transient compensation, and subsequent chronic dysregulation. Nevertheless, because the analysis was based on whole-blood transcriptomic data, repeated identification of *ALAS2* may also reflect changes in erythroid-cell proportion, reticulocyte abundance, anemia-associated compensation, or generalized stress erythropoiesis rather than an ITP-specific driver alone. Thus, *ALAS2* should currently be regarded as a biologically meaningful but exploratory marker of stage-related hematopoietic adaptation in ITP.

The transition from acute to chronic ITP is biologically plausible in light of current understanding of disease immunopathology. Acute ITP is often dominated by inflammatory activation, cytokine release, and autoantibody production, whereas chronic ITP increasingly involves sustained immune dysregulation.[30–32] The PD-1 pathway has been shown to regulate CTL activity, offering a new direction for immunomodulatory therapy.[10] Emerging treatments such as TPO-RAs, spleen tyrosine kinase (*SYK*) inhibitors, and FcγR inhibitors are under development, although monoclonal antibodies (e.g., rituximab) may induce adverse effects like hypogammaglobulinemia.[11] Despite advances in understanding immune phenomena and thrombopoietin biology, the genetic regulatory mechanisms of ITP remain to be fully elucidated. This study employs bioinformatics approaches to analyze differential gene expression and signaling pathways across distinct pathological stages, aiming to provide a theoretical foundation for targeted therapies.

An elegant study design is required to resolve these issues. Regarding *IL1R2*, it plays a key role as a decoy receptor for IL-1. This pathway modulates IL-1–driven downstream signals, influencing the balance of inflammatory mediators.[33,34] We found that *FCGR2B* suppresses B-cell receptor signaling, immune-complex responses, and autoantibody amplification.[35–37] Impaired *FCGR2B* function is associated with exaggerated humoral immunity and enhanced inflammatory cytokine production.[38–40] High *TREM1* expression on myeloid cells amplifies innate immune responses by triggering cytokine release.[41–43] The *FCGR2B–TREM1–IL1R2* axis identified here may therefore represent an ITP-relevant configuration of a broader autoimmune inflammatory module. In acute ITP, reduced inhibitory *FCGR2B* together with altered *TREM1*/*IL1R2* signaling may reflect a shift from immune restraint toward self-amplifying inflammatory platelet injury. Because *TREM1* occupies an upstream amplification position in innate inflammatory signaling, it may also represent a plausible immunomodulatory target for limiting excessive myeloid activation and cytokine escalation in active ITP.

Another key acute-phase feature was dysregulation of lipid and energy metabolism. *ACSL1*, which mediates long-chain fatty acid esterification and mitochondrial β-

IN PRESS

oxidation, was downregulated in ACU relative to CHR.[44] Because *ACSL1* is involved in macrophage lipid handling, inflammatory responses, and phospholipid remodeling, its reduction may contribute to metabolic imbalance and abnormal macrophage polarization during acute disease.[45–47] This interpretation is supported by coordinated changes in genes such as *PYGL*, *DGAT2*, *NCOA1*, and *TALDO1*, which collectively suggest impaired glycogenolysis, altered triglyceride synthesis, disturbed energy metabolism, and weakened antioxidant capacity.[48–50] These findings support the concept that acute ITP is associated not only with immune activation but also with substantial metabolic reprogramming. Such pathways may have therapeutic implications, as correction of immunometabolic imbalance could theoretically help dampen inflammatory effector responses and improve immune homeostasis.

In addition to immune and metabolic perturbations, several acute-phase changes pointed to coagulation and platelet-related dysfunction. Downregulation of *MME* and *LYN* may contribute to hemorrhagic tendency through combined effects on immune signaling, platelet activation, and inflammatory regulation.[51–53] Altered expression of *BASP1*, *MYADM*, *ASAP1*, *SORL1*, and *NIBAN1* further supports the presence of inflammatory activation, abnormal myeloid differentiation, dyslipidemia, and coagulation-associated disturbance during ACU.[54–56] Although many of these genes have not previously been studied in ITP in detail, their combined transcriptional pattern is compatible with a highly inflammatory, metabolically stressed, and hematopoietically unstable acute state.

The progressive/remission phase appeared to be characterized by partial compensatory responses rather than simple normalization. Upregulation of *VNN1*, *FBLN1*, *KLHL22*, and *SMOX* suggests activation of oxidative stress regulation, extracellular matrix remodeling, and compensatory hematopoietic or immune-modulatory mechanisms.[57–59] In particular, *VNN1* and its interaction with *VNN3* may reflect redox adaptation and modulation of local inflammatory tone, whereas *KLHL22* may support proliferative recovery and immune adjustment. Importantly, oxidative stress-related genes such as *VNN1* and *SMOX* may be more than passive markers of tissue stress. *VNN1* has been linked to redox-sensitive inflammatory regulation and epithelial or immune stress responses, while *SMOX* promotes polyamine catabolism and can generate hydrogen peroxide and other reactive byproducts that influence inflammatory signaling, cellular injury, and immune-cell behavior. In autoimmune progression, persistent activation of such oxidative pathways may contribute to a feed-forward loop in which inflammation induces redox imbalance, and redox imbalance in turn sustains immune dysregulation a

nd delayed resolution. Thus, the increased expression of *VNN1* and *SMOX* in PRO may indicate an intermediate state of ongoing autoimmune activity coupled to compensatory antioxidant or repair responses, rather than simple remission alone. Rather than representing complete restoration of homeostasis, the PRO stage may therefore reflect an intermediate transcriptional state in which inflammatory injury is being counterbalanced by metabolic and reparative programs. From a translational standpoint, this raises the possibility that oxidative stress regulators may serve not only as stage-associated biomarkers but also as adjunct therapeutic targets for interrupting redox-driven amplification of autoimmune inflammation.

The chronic stage showed a different molecular profile, with stronger evidence of persistent hematopoietic stress, altered erythroid biology, and immune adaptation. Downregulation of *HBG1* together with persistent *ALAS2* dysregulation suggests impaired hemoglobin synthesis, chronic erythropoietic dysfunction, and disturbed oxygen-related metabolism.[60–62] These changes are biologically plausible in a setting of prolonged immune dysregulation and sustained marrow stress. The chronic-phase upregulation of *OTULIN*, *TAF9B*, and *SLC23A2* may represent compensatory anti-inflammatory, anti-oxidative, and cell-survival programs.[63–65] In particular, *SLC23A2*, which encodes the vitamin C transporter SVCT2, may support antioxidant protection, hematopoietic maintenance, and immune modulation through regulation of intracellular vitamin C availability. Its increased expression in CHR is compatible with an adaptive response to persistent oxidative and inflammatory stress, although the functional relevance of this pathway in chronic ITP remains to be experimentally validated.[66,67] These chronic-stage antioxidant and survival-associated signatures may also have therapeutic implications, as they suggest that redox-supportive or immune-restorative strategies could be explored to mitigate long-term inflammatory stress and hematopoietic dysfunction.

IN PRESS

Published by Tehran University of Medical Sciences (http://ijaai.tums.ac.ir)

Overall, our findings indicate that ITP progression involves both shared autoimmune hematologic mechanisms and stage-dependent molecular features. The genes identified here should therefore be regarded as candidate rather than clinically validated biomarkers. Their potential value lies in their stage-specific expression patterns, which may help distinguish acute, progressive, and chronic ITP and thereby support disease stratification, prognosis assessment, and treatment monitoring. In particular, *ALAS2*, *VNN1*, and *SLC25A37* merit further validation in independent cohorts using qPCR or protein-based assays. The pathways highlighted by these DEGs, especially those related to *FCGR2B*, *IL1R2*, *TREM1*, *ACSL1*, and *ALAS2*/*HBG1*, may also provide mechanistic insight and suggest potential therapeutic targets. Importantly, the concordance of *FCGR2B*-, *IL1R2*-, and *TREM1*-related changes with known immune-regulatory mechanisms in other autoimmune diseases strengthens the biological plausibility of our findings and suggests that ITP may share a conserved inflammatory circuitry while retaining stage-specific transcriptional organization. More specifically, our results support the idea that inhibitory immune signaling, innate inflammatory amplification, oxidative stress adaptation, and immunometabolic remodeling may together constitute a set of stage-relevant immunomodulatory axes. Although these pathways cannot yet be considered validated treatment targets based on transcriptomic evidence alone, they provide a rational framework for future therapeutic exploration, including strategies aimed at restoring immune tolerance, limiting myeloid inflammatory activation, and reducing redox-driven tissue injury.

Several limitations should be acknowledged. First, the potential confounding effects of patient medications (such as glucocorticoids) on the identified transcriptomic signatures could not be ruled out. Second, the sample size was relatively small, particularly for the PRO stage (n=4). Third, although we identified potential hub genes and key biological pathways, these findings were based purely on bioinformatic analysis of public datasets and lack direct experimental validation in clinical samples. Future prospective studies with larger, well-phenotyped cohorts are required to confirm the diagnostic and prognostic value of these candidate biomarkers.

STATEMENT OF ETHICS

All analyses were based on previously published studies; therefore, no ethical approval or patient consent was required.

FUNDING

This study was supported by the General Program of the China Postdoctoral Science Foundation (No. F119290147) and the Guangdong Basic and Applied Basic Research Foundation—Youth Fund Project (No. 2021A1515110575).

CONFLICT OF INTEREST

The authors declare no conflicts of interest.

ACKNOWLEDGMENTS

Not applicable.

DATA AVAILABILITY

The dataset analyzed during the current study is available in the Gene Expression Omnibus repository (accession number GSE23754).

AI ASSISTANCE DISCLOSURE

AI tools were not used in the preparation of this manuscript.

REFERENCES

1. Krieg A, Krieg S, Heuser A, Laverenz U, Istrate VA, Schott M, et al. Exploring the spectrum of comorbidities associated with primary aldosteronism: insights from a large real-world case-control study. Biomedicines. 2024;12(11):2479.
2. Araujo-Castro M, Ruiz-Sández JG, Parra Ramírez P, Martín Rojas-Marcos P, Aguilera-Saborido A, Gómez Cerezo JF, et al. Screening and diagnosis of primary aldosteronism. Endocrine. 2024;85(1):99–121.
3. Monticone S, D'Ascenzo F, Moretti C, William TA, Veglio F, Gaita F, et al. Cardiovascular events and target organ damage in primary aldosteronism compared with essential hypertension: a systematic review and meta-analysis. Lancet Diabetes Endocrinol. 2018;6(1):41–50.
4. Demirkiran A, Everaars H, Elitok A, van de Ven PM, Smulders YM, Dreijerink KM, et al. Hypertension with primary aldosteronism is associated with increased carotid

IN PRESS

intima-media thickness and endothelial dysfunction. J Clin Hypertens. 2019;21(7):932–941.
5. Muiesan ML, Paini A, Rosei CA, Bertacchini F, Aggiusti C, Rizzoni C, et al. Hypertension and target organ damage. In: Encyclopedia of Endocrine Diseases. 2019:406–414.
6. Brobak KM, Halvorsen LV, Aass HCD, Søraas CL, Aune A, Olsen E, et al. Novel biomarkers in patients with uncontrolled hypertension with and without kidney damage. Blood Press. 2024;33(1).
7. Xing J, Lai C, Liu X, Zhao J, Qi J, Hu F. Changes of high sensitivity C-reactive protein and interleukin-6 in patients with hypertension and target organ damage and its significance. Chin Remedies Clin. 2015.
8. Peng QU. Correlation study of high-sensitivity C-reactive protein with risk factors and target organ damage in hypertensive patients. Chin J Postgrad Med. 2011.
9. Chinese Society of Endocrinology. Expert consensus on the diagnosis and treatment of primary aldosteronism (2020 edition). Chin J Endocrinol Metab. 2020;36(9):727–736.
10. Chinese Hypertension League. Chinese guidelines for the prevention and treatment of hypertension (revised edition 2024). Chin J Hypertens. 2024;32(7):603–700.
11. Lang RM, Badano LP, Mor-Avi V, Afilalo J, Armstrong A, Ernande L, et al. Recommendations for cardiac chamber quantification by echocardiography in adults. J Am Soc Echocardiogr. 2015;28(1):1–39.e14.
12. Touboul PJ, Hennerici MG, Meairs S, Adams H, Amarenco P, Bornstein N, et al. Mannheim carotid intima-media thickness and plaque consensus. Cerebrovasc Dis. 2012;34(4):290–296.
13. Levey AS, Stevens LA, Schmid CH, Zhang YL, Castro AF, Feldman HI, et al. A new equation to estimate glomerular filtration rate. Ann Intern Med. 2009;150(9):604–612.
14. Levin A, Ahmed SB, Carrero JJ, Foster B, Francis A, Hall RK, et al. KDIGO 2024 clinical practice guideline for the evaluation and management of chronic kidney disease. Kidney Int. 2024;105(4):684–701.
15. Ferreira NS, Tostes RC, Paradis P, Schiffrin EL. Aldosterone, inflammation, immune system, and hypertension. Am J Hypertens. 2021;34(1):15–27.
16. 16. Barrera-Chimal J, Jaisser F. Vascular and inflammatory mineralocorticoid receptors in kidney disease. Acta Physiol (Oxf). 2020;228(2):e13390.
17. 17. Lai LQ, Gu Y. Research progress on chronic kidney injury in primary aldosteronism. J Intern Med Theory Pract. 2023;18(03):211–214.
18. 18. Cui T, Wang J, Shui W, Kang C, Zhang Z, Zan Y, et al. Interleukin-6 and C-reactive protein with left ventricular geometry and function in obstructive sleep apnea and pre-hypertension. Echocardiography. 2022;39(2):286–293.
19. Xu Z, Yang S, Tan Y, Zhang Q, Wang H, Tao J, et al. Inflammation in cardiovascular-kidney-metabolic syndrome: mechanisms. Mol Cell Biochem. 2025.
20. Wu VC, Chan CK, Chueh JS, Chen YM, Lin YH, Chang CC, et al. Kidney tubular function in primary aldosteronism after treatment. J Am Heart Assoc. 2023;12(4):e028146.
21. Weber BN, Giles JT, Liao KP. Shared inflammatory pathways of rheumatoid arthritis and atherosclerotic cardiovascular disease. Nat Rev Rheumatol. 2023;19(7):417–428.
22. Ahmad MI, Chevli P, Mirzai S, Spitz JA, Sharma G, Lima J, et al. Association between *CKM* syndrome, inflammatory biomarkers, and outcomes. Atherosclerosis. 2025;410:120521.
23. van der Heijden C, Keating ST, Groh L, Joosten LA, Netea MG, Riksen NP. Aldosterone induces trained immunity via fatty acid synthesis. Cardiovasc Res. 2020;116(2):317–328.
24. Erratum. Immune microenvironment profiling of primary aldosteronism. J Hypertens. 2025;43(9):1603.
25. Nowotny HF, Zheng T, Seiter TM, Ju J, Schneider H, Kroiss M, et al. Sex-dependent modulation of immune cells and microbiome in primary aldosteronism. Front Immunol. 2024;15:1428054.
26. Pretorius E, du Plooy JN, Bester J. A comprehensive review on eryptosis, erythrocytes, and oxidative stress in inflammation. Biomolecules. 2016;6(3):31.
27. Zhou M, Guo R, Wang YF. Application of weighted gene coexpression network analysis to identify key modules and hub genes in systemic juvenile idiopathic arthritis. Biomed Res Int. 2021;2021:9957569.
28. Sun H. Identification of regulatory factors and prognostic markers in amyotrophic lateral sclerosis. Antioxidants (Basel). 2022;11(2):303.
29. Sommer N, Fabian F. Mitochondrial respiration in peripheral blood mononuclear cells negatively correlates with disease severity in pulmonary arterial hypertension. J Clin Med. 2022;11(14):4132.
30. Cooper N, Ghanima W. Immune thrombocytopenia. N Engl J Med. 2024;390(10):945–957.
31. Liu *XG*, Hou Y, Hou M. How we treat primary immune thrombocytopenia in adults. J Hematol Oncol. 2023;16(1):4.

IN PRESS

32. Semple JW, Schifferli A, Cooper N. Immune thrombocytopenia: pathophysiology and impacts of romiplostim treatment. Blood Rev. 2024;67:101222.
33. Molgora M, Barajon I, Mantovani A, Garlanda C. Regulatory role of IL-1R2 in the control of inflammation and immunity. Front Immunol. 2018;9:1838.
34. Mantovani A, Dinarello CA, Molgora M, Garlanda C. Interleukin-1 and related cytokines in the regulation of inflammation and immunity. Immunity. 2019;50(4):778–795.
35. Espeli M, Smith KGC, Clatworthy MR. FcγRIIB and autoimmunity. Immunol Rev. 2016;269(1):194–211.
36. Bournazos S, Ravetch JV. Fcγ receptor pathways during active and passive immunization. Immunity. 2017;47(2):224–233.
37. Honda S, Zhang Y, Minhas V. FcγRIIB controls antigen-independent B cell development and prevents autoimmunity. J Exp Med. 2017;214(2):567–581.
38. Su K, Yang H. Expression profile of FcγRIIb on leukocytes and its dysregulation in systemic lupus erythematosus. J Immunol Res. 2017;2017:8468146.
39. Anania JC, Chenoweth AM, Wines BD, Hogarth PM. The human FcγRII (CD32) family of leukocyte Fc receptors in health and disease. Front Immunol. 2019;10:464.
40. Mkaddem SB, Benhamou M, Monteiro RC. Understanding Fc receptor involvement in inflammatory diseases: from mechanisms to new therapeutic tools. Front Immunol. 2019;10:811.
41. Tammaro A, Derive M, Gibot S. TREM-1 and its potential ligands in non-infectious diseases: from biology to clinical perspectives. Pharmacol Ther. 2017;177:81–95.
42. Kuai J, Gregory B, Hill A. TREM1-positive macrophages define a pathogenic inflammatory state in human inflammatory disease. Front Immunol. 2021;12:711954.
43. Tessarz AS, Cerwenka A. The TREM-1/DAP12 pathway. Immunol Lett. 2008;116(2):111–116.
44. Misheva M, Kotzamanis K, Davies LC. Oxylipin metabolism is controlled by mitochondrial β-oxidation during bacterial inflammation. Nat Commun. 2022;13:139.
45. Roeland J. Long-chain acyl-CoA synthetase role in sepsis and immunity: perspectives from transcriptome datasets and literature. Front Immunol. 2019;10:2410.
46. Rubinow KB, Wall VZ, Nelson J. Acyl-CoA synthetase 1 is induced by Gram-negative bacteria and lipopolysaccharide and is required for phospholipid turnover in stimulated macrophages. J Biol Chem. 2013;288(14):9957–9970.
47. Al-Rashed F, Thoma R, Al-Roub A. LPS induces GM-CSF production via long-chain acyl-CoA synthetase 1. Molecules. 2020;25(19):4709.
48. Chitraju C, Walther TC, Farese RV Jr. Triglyceride synthesis enzymes *DGAT1* and *DGAT2* have distinct and overlapping functions in adipocytes. J Lipid Res. 2019;60(6):1112–1120.
49. Matias MI, Yong *CS*. Regulatory T cell differentiation is controlled by AKG-induced mitochondrial metabolism and lipid homeostasis. Cell Rep. 2021;37(6):109911.
50. Mornata F, Pepe G, Sfogliarini C, et al. Reciprocal interference between NRF2 and LPS signaling pathways on the immune-metabolic phenotype of peritoneal macrophages. Pharmacol Res Perspect. 2020;8:e00638.
51. Zhi H, Dai J, Liu J. Platelet activation and thrombus formation over IgG immune complexes requires integrin αIIbβ3 and Lyn kinase. PLoS One. 2015;10(8):e0135738.
52. Zhang J, Chang J, Beg MA. Na+/K+-ATPase suppresses LPS-induced pro-inflammatory signaling through Lyn. iScience. 2022;25:104963.
53. Nortier JL, Remiche G. Antenatal membranous nephropathy and type 2 (axonal) Charcot-Marie-Tooth with mutations in the metallo-membrane endopeptidase gene. Kidney Int Rep. 2021;6:1981–1986.
54. Xu S, Tang L, Liu Z. Hypoxia-related lncRNA correlates with prognosis and immune microenvironment in lower-grade glioma. Front Immunol. 2021;12:731048.
55. Desterke C, Bennaceur-Griscelli A, Turhan AG. *EGR1* dysregulation defines an inflammatory and leukemic program in human-aged hematopoietic stem cells. Stem Cell Res Ther. 2021;12:419.
56. Xu Y, Chen D, Shen L. Identification and mechanism of the PD-1/PD-L1 genomic signature *SORL1* as a protective factor in bladder cancer. Front Genet. 2021;12:736158.
57. Wang N, Qin X. Plasma vanin-3 is associated with gastrointestinal acute graft-versus-host disease in mice. J Inflamm (Lond). 2018;15:1–7.
58. Ferreira DW, Goedken MJ, Rommelaere S. Enhanced hepatotoxicity by acetaminophen in vanin-1 knockout mice is associated with deficient proliferative and immune responses. Biochim Biophys Acta. 2016;1862(4):662–669.
59. Zhou XA, Zhou J, Zhao L. *KLHL22* maintains PD-1 homeostasis and prevents excessive T cell suppression. Proc Natl Acad Sci U S A. 2020;117(45):28239–28250.
60. Li C, Georgakopoulou A, Mishra A. In vivo HSPC gene therapy with base editors allows efficient reactivation of fetal γ-globin in β-YAC mice. Blood Adv. 2021;5(4):1122–1135.

IN PRESS

61. Heshusius S, Heideveld E, von Lindern M. *CD14*$^{+}$ monocytes repress γ-globin expression at early stages of erythropoiesis. Sci Rep. 2021;11:1507.
62. Zhou G, Zhang H, Lin A. Multi-omics analysis in β-thalassemia using an *HBB* gene-knockout human erythroid progenitor cell model. Int J Mol Sci. 2022;23:2807.
63. Weinelt N, van Wijk SJL, et al. Ubiquitin-dependent and -independent functions of *OTULIN* in cell fate control and beyond. Cell Death Differ. 2021;28:493–504.
64. Gu W, Chen P, Ren P. Downregulation of *TAF9B* by miR-7-5p inhibits progression of osteosarcoma. Onco Targets Ther. 2021;14:2917–2927.
65. Hou H, Zhang Y, Wu H. Impact of *SLC23A1* and *SLC23A2* polymorphisms on risk of preeclampsia in a Chinese Han population. J Nutr Sci Vitaminol (Tokyo). 2022;68:368–374.
66. Oyarce K, Campos-Mora M, Gajardo-Carrasco T. Vitamin C fosters in vivo differentiation of *CD4*$^{+}$*FOXP3*$^{-}$ T cells into *CD4*$^{+}$*FOXP3*$^{+}$ regulatory T cells but impairs graft survival. Front Immunol. 2018;9:112.
67. Przybylo M, Langner M. Physiological and cellular homeostasis of ascorbate. Cell Mol Biol Lett. 2020;25:32.

IN PRESS